Quantum critical point and intermediate valence fluctuations in CeRu$_{2-x}$Co$_x$Ge$_2$

Swati Pandey,[1] Vasudeva Siruguri,[1,*] and Rajeev Rawat[2]

[1]*UGC-DAE Consortium for Scientific Research Mumbai Centre, BARC Campus, Mumbai 400085, India*
[2]*UGC-DAE Consortium for Scientific Research, University Campus, Khandwa Road, Indore 452001, India*

A detailed study of low-temperature properties across the series CeRu$_{2-x}$Co$_x$Ge$_2$ ($0 \leqslant x \leqslant 2$) using magnetic susceptibility $\chi(T)$, isothermal magnetization $M(H)$, heat capacity $C(T)$, and electrical resistivity $\rho(T)$ is presented. Using doping as a tuning parameter, a crossover from a Ruderman-Kittel-Kasuya-Yosida (RKKY) dominated region ($0 \leqslant x \leqslant 1$) to a Kondo dominated region ($x \geqslant 1.5$) is evident. $\chi(T)$ and $\rho(T)$ curves, analyzed in terms of theoretical models proposed by Sales and Freimuth for the Co ($x \geqslant 1.5$) rich compounds, suggest an intermediate valence state of the Ce ion. The intricate balance between the competing RKKY and Kondo effect is attributed to the volume change upon Co substitution, owing to its smaller ionic size, which enhances the hybridization between $4f$ and conduction electrons. A quantum critical point (QCP) in the (T, x) phase diagram is reached for the critical concentration ($x_c \sim 1.5$) where the competing RKKY and Kondo energy scales tend to zero. Deviation in $\chi(T)$, $C(T)$, and $\rho(T)$ from Fermi-liquid behavior is observed in the vicinity of the QCP and the former is seen to recover with the application of magnetic field. Further support for the quantum criticality comes from the universal scaling behavior of $M(H)$, $\chi(T)$, and $\rho(T)$ data for $x_c \sim 1.5$. Also, the valence fluctuations in the vicinity of the compound showing non-Fermi-liquid behavior may suggest the possible role of valence fluctuations in the QCP, which makes the present series an interesting case.

I. INTRODUCTION

Rare-earth intermetallic compounds with strongly correlated f electrons are studied with great interest due to their novel properties. Among them, the cerium-based ternary intermetallic compounds CeT_2X_2 family ($T =$ transition metal and $X =$ Si or Ge) has gained a special interest due to the presence of competing ground states like coexistence of magnetic ordering and superconductivity [1], Kondo effect [2], quantum criticality [3], heavy fermion superconductivity [1], and intermediate valence fluctuation [4–6]. Depending on the environment around the Ce atom, the $4f$ shell becomes unstable and results in hybridization between the localized $4f$ electron states and conduction electron states which are associated with the formation of many electron states near the Fermi level [7]. The ground states of such compounds are mainly determined by a competition between the intersite long-range Ruderman-Kittel-Kasuya-Yosida (RKKY) interaction (denoted by T_{RKKY}) and on-site Kondo interaction (denoted by T_K) and are well described by Doniach's necklace model [8]. According to this model, both of these interactions depend on the exchange integral J_{cf} between the $4f$ localized moments and conduction electrons. For small values of J_{cf}, RKKY interaction dominates (where $T_{\mathrm{RKKY}} \propto J_{cf}{}^2$) and the system orders magnetically while for a large value of J_{cf} Kondo interaction dominates [$T_K \propto \exp(-1/J_{cf})$], leading to a nonmagnetic ground state. However, at a critical value of J_{cf}, reached via some nonthermal parameters such as magnetic field, pressure, and chemical doping, a quantum critical point (QCP) is observed and is reported for various

U and Ce based heavy fermion compounds [9–12]. Such QCPs often manifest in the form of non-Fermi-liquid (NFL) behavior in the physical properties through deviations from the usual Fermi-liquid (FL) behavior at low temperatures: $C/T \sim \chi \sim$ constant and $\rho(T) \sim T^2$.

Thermodynamic and transport studies on CeT_2X_2 compounds reveal that varying the "transition metal" T causes a variation in strength of J_{cf} resulting in different possible ground states; for example, CeCu$_2$Si$_2$ is a well-known heavy fermion superconductor [1], and CeNi$_2$Si$_2$ shows a valence fluctuating state [13], whereas CeRu$_2$Si$_2$ [14,15] presents a heavy fermion ground state. Among CeT_2X_2, most of the compounds have an antiferromagnetic (AFM) ground state. In contrast, however, CeRu$_2$Ge$_2$ is a unique one having a ferromagnetic (FM) ground state. With decrease in temperature, it first undergoes a paramagnetic (PM) to AFM transition at $T_N = 8.5$ K and enters into an FM state below $T_C = 7.4$ K. The nature of the transition at T_N is of second order while the transition at T_C is of the first order [16–18]. Neutron-scattering studies performed by Loidl *et al.* [19] suggest the Kondo temperature (T_K) to be less than 2 K. On the other hand, CeCo$_2$Ge$_2$, based on x-ray photoemission spectroscopy studies, is suggested to be a possible heavy fermion intermediate valence fluctuating (IVF) compound with T_K of about 120 K [20,21]. However, a complete study confirming the ground state is still lacking.

Moreover, studies further suggest a QCP as a function of pressure or doping. Using pressure (P) and doping (x) as a tuning parameter, various studies on CeRu$_2$Ge$_2$ present a similar kind of (T, P) and (T, x) phase diagrams. Pressure dependent studies on CeRu$_2$Ge$_2$ [22–25] show the suppression of the magnetic order and lead to a heavy fermion nonmagnetic ground state for $P > 7.5$ GPa. A pressure induced QCP

*siruguri@csr.res.in
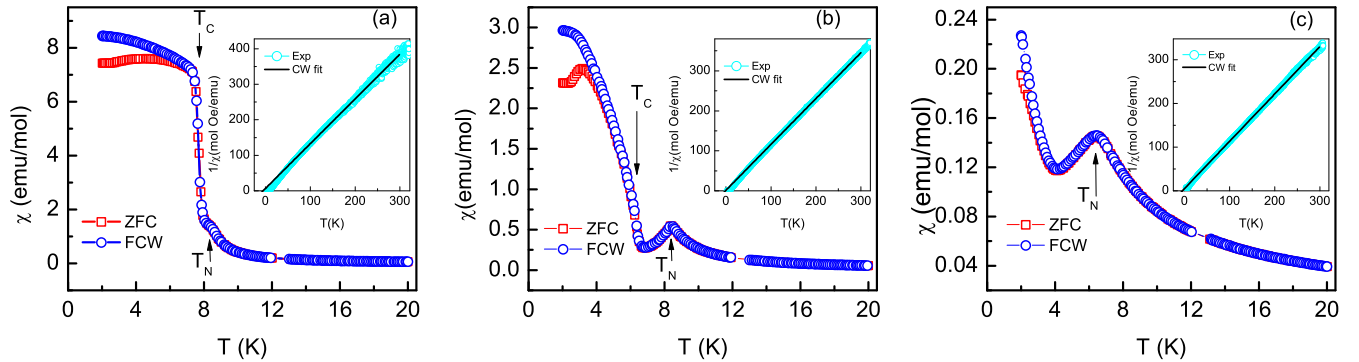
FIG. 1. Temperature-dependent magnetic susceptibility for $CeRu_{2-x}Co_xGe_2$ where (a) $x = 0$, (b) $x = 0.5$, and (c) $x = 1$, at $H = 100$ Oe. The inset shows inverse magnetic susceptibility along with CW fit.

is reported at a critical pressure $P_C \sim 8.7$ GPa. Similarly, doping smaller Fe at the Ru site in $CeRu_{2-x}Fe_xGe_2$ [26] and Si at the Ge site in $CeRu_2Ge_{2-x}Si_x$ [27] as a function of x resulted in a gradual change of the ground state from a RKKY dominated regime to a Kondo dominated regime. Also, a QCP in the (T, x) phase diagram for $CeRu_{2-x}Fe_xGe_2$ could be located at a critical concentration of $x_c \sim 0.9$ [26]. However, presently there is no consensus on the type of QCP present in the system. A study incorporating the inelastic neutron scattering suggested different scenarios related to the observed QCP in $CeRu_{2-x}Fe_xGe_2$ [28]. Additionally, in these studies, the valence of Ce across the series is seen to remain close to a value of $+3$ expected for a magnetic ion f^1. However, no superconducting transition either as a function of pressure or doping in $CeRu_2Ge_2$ is reported down to the lowest temperature measured, unlike the case of $CeCu_2Si_2$ [29] and $CeCu_2Ge_2$ [30].

A previous report [31] on the series $CeRu_{2-x}Co_xGe_2$ using structural and magnetotransport study established the role of unit-cell volume in deciding the ground state as a function of x. The present paper provides a detailed study of the crossover from a RKKY interaction (Ru rich; $0 \leqslant x \leqslant 1$) to a Kondo interaction (Co rich; $x \geqslant 1.5$) leading to a valence fluctuating state (for $x \geqslant 1.5$) resulting from a strong $4f$-conduction electron hybridization due to the change in unit-cell volume as a function of doping. A systematic study on temperature and field dependence of magnetic susceptibility, electrical resistivity, and heat capacity across the series $CeRu_{2-x}Co_xGe_2$ provides an additional emphasis on the IVF ($x \sim 1.5, 1.8$, and 2.0) and NFL nature ($x \sim 1.5$) of the compounds. We also show that magnetization and resistivity data exhibit universal scaling behavior indicating the proximity of $x_c \sim 1.5$ to the QCP. This paper is organized as follows: The physical properties of $CeRu_2Ge_2$, $CeRu_{1.5}Co_{0.5}Ge_2$, and $CeRuCoGe_2$ examined by magnetic susceptibility, heat capacity, and electrical resistivity are described in Sec. IIIA, and valence fluctuating phenomena for $CeRu_{0.5}Co_{1.5}Ge_2$, $CeRu_{0.2}Co_{1.8}Ge_2$, and $CeCo_2Ge_2$ are presented in Sec IIIB, while in Sec IIIC NFL behavior of $CeRu_{0.5}Co_{1.5}Ge_2$ close to the QCP is presented.

II. EXPERIMENTAL DETAILS

Details of sample preparation and x-ray diffraction (XRD) are given in Ref. [31]. The samples used for the present measurement belong to the same respective batch as used in

the earlier study. Magnetic susceptibility measurements were performed in the temperature range 2–300 K and in magnetic fields up to 90 kOe using a vibrating sample magnetometer based Quantum Design physical property measurement system (QD-PPMS). Electrical resistivity data used for the present paper are taken from Ref. [31] from measurements in the temperature range 1.6–300 K and in the presence of magnetic field up to 80 kOe using a standard dc four-probe technique. The heat-capacity data were collected in the temperature range 1.8–300 K and in magnetic fields up to 140 kOe employing adiabatic relaxation technique in the QD-PPMS equipped with a 14-T magnet.

III. RESULTS

A. $x = 0, 0.5$, and 1: Magnetic ground state

Figures 1(a)–1(c) show the magnetic susceptibility (M/H) as a function of temperature for $x = 0, 0.5$, and 1, measured under a magnetic field of 100 Oe. As shown in Fig. 1(a), the pure compound, $CeRu_2Ge_2$, shows two magnetic transitions, one at $T_N = 8.3$ K from a PM state to an AFM state and the second at $T_C = 7.6$ K from an AFM state to an FM state (marked by arrows), and they are in good agreement with previously reported results [16,17]. For $x = 0.5$, T_N remains unchanged while T_C shifts to 6.3 K. For $x = 1$, where Ru and Co are in equal proportion, T_N shifts to 6.5 K while there is no evidence of T_C down to 2 K. A small bifurcation between zero-field cooled and field cooled curves below T_C indicates the soft FM nature of the compound. Inverse magnetic susceptibility (H/M) as a function of temperature (shown as an inset in the respective curves) in the temperature range 100–300 K is fitted with a modified Curie-Weiss (CW) law $\chi(T) = \chi_0 + C/(T - \theta_P)$, where θ_P is the PM Curie temperature and C is the Curie constant. The calculated effective moment $\mu_{\rm eff}$ as given in Table I is found to be close to the theoretical value

TABLE I. Values of paramagnetic Curie temperature θ_P (K), effective moment $\mu_{\rm eff}$ (μ_B), and Kondo temperature T_K (K) for different x obtained from the magnetic susceptibility.

x	$-\theta_P$	$\mu_{\rm eff}$	T_K
0	5.1	2.52	2.5
0.5	5.3	2.64	2.6
1	5.8	2.72	2.9
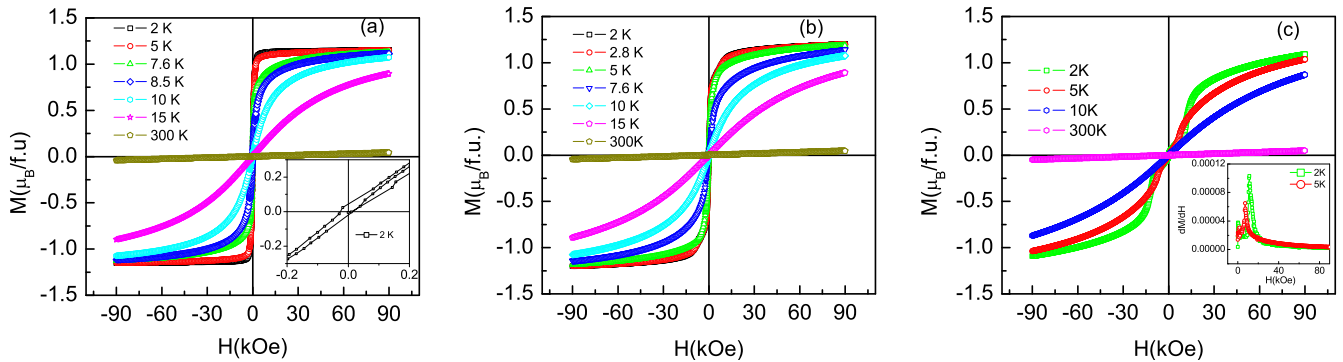
FIG. 2. Isothermal magnetization for (a) $x = 0$, (b) $x = 0.5$, and (c) $x = 1$ in CeRu$_{2-x}$Co$_x$Ge$_2$. The inset of (a) shows an enlarged view of the $M(H)$ curve at 2 K near the origin, (c) Derivative of the virgin curves of 2 and 5 K.

of $2.54\mu_B$ for Ce^{3+} ions. Also, θ_P is related to the Kondo temperature by $T_K = |\theta_P|/2$ [32]. The obtained values of T_K and θ_P are given in Table I. Moreover, increase in the values of θ_P with x suggests an increase in $4f$-conduction electron hybridization.

Figures 2(a)–2(c) show the isothermal magnetization $M(H)$ curves at different temperatures for the compositions $x = 0$, 0.5, and 1. For CeRu$_2$Ge$_2$, there is a small hysteresis of ~39 Oe at 2 K [see inset of Fig. 2(a)] and it shows a saturation behavior at a few kilo-oersted, confirming the FM nature of the compound. The magnetization data extrapolated from the higher-field region, towards zero field, gives the spontaneous magnetization of $1.13\,\mu_B$/Ce. However, the observed saturation magnetization for $x = 0$ at 2 K in the field of 90 kOe is $M_{\text{sat}} = 1.15\,\mu_B$/Ce, which is less than the theoretical value of $2.14\,\mu_B$/Ce, suggesting a crystal-field split ground state. The behavior of $M(H)$ curves for $x = 0.5$ is similar to the parent compound with a slight rounding off across the saturation at low temperatures. For $x = 1$, a field induced metamagnetic transition is clearly observable at 2- and 5-K temperatures with the value of the critical field being $H_C = 11$ kOe at 2 K and $H_C = 7$ kOe at 5 K, suggesting the AFM nature, and is in line with the earlier magnetotransport study [31].

The results of heat capacity as a function of temperature between 1.8 and 40 K for $x = 0$, 0.5, and 1 measured under zero field are presented in Fig. 3. Two magnetic transitions for $x = 0$ appear at $T_C = 7.5$ K and $T_N = 8.3$ K (marked by arrows in the inset of Fig. 3). The peak positions for $x = 0.5$ move to $T_C = 6.3$ K and $T_N = 8$ K. However, only a broad AFM transition at $T_N = 6.6$ K could be observed for $x = 1$. All the transition temperatures are in line with the magnetization and resistivity data (see the section on resistivity below).

The temperature-dependent electrical resistivity [$\rho_{(T)}/\rho_{(50\,\text{K})}$] normalized at 50 K for $x = 0$, 0.5, and 1 measured under zero magnetic field is shown in Fig. 4. The resistivity curve for $x = 0$ shows a feature at $T_N = 8.5$ K and at $T_C = 7.5$ K, below which a sharp drop occurs due to a reduction in spin disorder scattering. For $x = 0.5$, the resistivity first increases with decreasing temperature, then shows a maximum at 8.5 K, followed by a small hump at 6 K and a sharp decrease below it. However, only a single AFM transition at $T_N = 6.5$ K could be observed for $x = 1$. The value of magnetic transitions matches well with the magnetization and heat-capacity data.

The minimum in resistivity suggests the role of increasing strength of Kondo scattering and it increases with increase in Co concentration.

B. $x = 1.5$, 1.8, and 2: Nonmagnetic and intermediate valence fluctuating ground states

As is evident from Figs. 5(a)–5(c), no features related to the magnetic ordering could be observed down to 2 K in the magnetic susceptibility $\chi(T)$ curves for the concentrations $x \geqslant 1.5$. The Kondo effect starts dominating with the increase in Co substitution which results in the suppression of the magnetic ordering. A broad maximum for $x = 1.8$ and 2 [Figs. 5(b) and 5(c)] could be observed at around 65 and 120 K, respectively. This broad maximum with the weak temperature dependence of susceptibility of the order of 10^{-3} emu/mole Ce atom manifests the nonmagnetic nature of the given compounds and is often recognized as the feature related to an intermediate valence fluctuation, commonly observed for Ce and Yb based compounds [5,33]. A sharp Curie-like rapid increase at low temperatures in $\chi(T)$ curves may arise due to the presence of stable Ce^{3+} ions at the grain boundaries or some other defect. To further interpret this data,
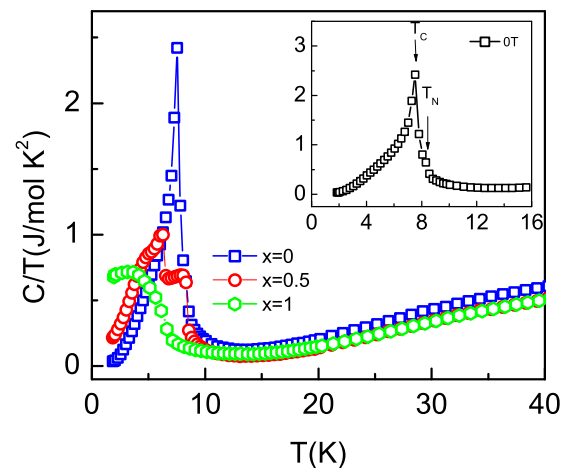
FIG. 3. Temperature-dependent heat capacity for concentration $x = 0$, 0.5, and 1 represented as C/T vs T measured in zero magnetic field. The inset shows a magnified view of the $x = 0$ curve where transitions are indicated by arrows.
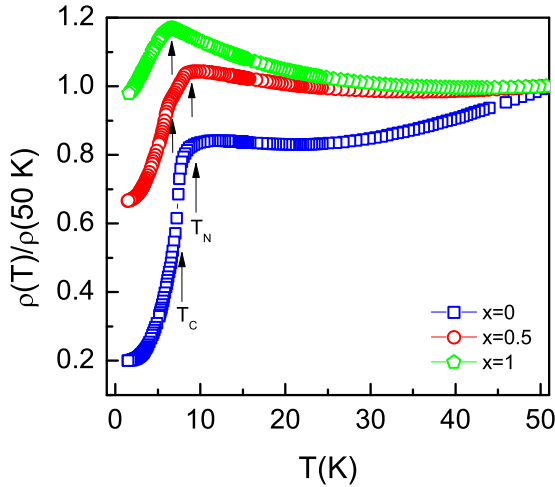
FIG. 4. The normalized electrical resistivity [$\rho_{(T)}/\rho_{(50\,K)}$] vs temperature measured under zero field for $x = 0$, 0.5, and 1. Arrows indicate magnetic transition.

we have fitted our magnetic susceptibility data with a two level ionic interconfiguration fluctuation (ICF) model given first by Hirst [34] and later modified by Sales and Wohlleben [35] and Franz *et al.* [36]. According to the ICF model, the rare-earth Ce fluctuates between a nonmagnetic $4f^0$ ($J = 0$ and $\mu_{eff} = 0$) and a magnetic $4f^1$ ($J = 5/2$ and $\mu_{eff} = 2.54$) configuration with a rate proportional to spin-fluctuation temperature T_{SF}, and is given by the following equation:

$$\chi(T) = (1-n)\left(\frac{N}{3k_B}\right)\frac{\left\{\mu_1^2 \nu(T) + \mu_2^2[1-\nu(T)]\right\}}{\sqrt{T^2 + T_{SF}^2}}$$

$$+ n\left[\frac{C}{T-\theta}\right] + \chi_0, \qquad (1)$$

$$\nu(T) = \frac{2J_1 + 1}{(2J_1 + 1) + (2J_2 + 1)\exp\left(\frac{-E_{ex}}{k_B\sqrt{(T^2 + T_{SF}^2)}}\right)}, \qquad (2)$$

where μ_1, μ_2 and $(2J_1 + 1)$, $(2J_2 + 1)$ are the respective effective moments and degeneracies of the E_1 and E_2 energy states corresponding to $4f^0$ and $4f^1$ states. $E_{ex} = E_1 - E_2$

TABLE II. Parameters obtained from the fitting of the magnetic susceptibility data with the ICF model.

X	E_{ex}/k_B (K)	T_{SF} (K)	$\chi(0)$ (emu/mol)	Ce valence at 300 K
1.5	48	44	6.1×10^{-4}	3.16
1.8	182	56	6.7×10^{-4}	3.21
2	258	92	8.4×10^{-4}	3.24

is the interconfigurational excitation energy. Here, $\nu(T)$ is the fractional occupation of nonmagnetic configuration $4f^0$. In order to take care of the contribution from a small amount of magnetic Ce^{3+} ions which are stabilized on grain boundaries or lattice defects, we have added a term $n[\frac{C}{T-\theta}]$ in Eq. (1), where the Curie term gives a contribution from stable Ce^{3+} in a total of n atoms per mole and χ_0 is the PM contribution due to conduction electrons and a diamagnetic contribution due to core electrons. As shown in Figs. 5(a)–5(c), fit of the susceptibility data for $x = 1.5$, 1.8, and 2 represented by the solid line based on the ICF model gives a good agreement with the experimental data. The parameters obtained from the ICF model fitting are given in Table II and the values are typical for the Ce based (IVF) compounds [37]. The values of E_{ex} and T_{SF} are found to increase with increasing x, suggesting the increase in valence fluctuation. Valency of the Ce ion at 300 K is calculated using Eq. (2) and is listed in Table II.

The field dependent magnetization $M(H)$ measured at selected temperatures is shown in Figs. 6(a)–6(c). The values of saturation magnetization at the highest measured field get drastically reduced for $x \geqslant 1.5$. The reduced moment value further suggests that the magnetic moments get compensated by the Kondo effect with increasing values of x and is in agreement with the IVF behavior for the Co rich compounds. Similar behavior is also observed in the other Ce based compounds CeT_2Si_2 ($T =$ Ru, Pd, Os, Pt, Ir) [38,39].

Figure 7(a) shows a plot of C/T versus T curves for $x = 1.5$, 1.8, and 2. Below 10 K, C/T for $x = 1.5$ shows a logarithmic temperature dependence suggesting the NFL behavior (described in Sec. IIIC) while for $x = 1.8$ and 2 it shows a linear temperature dependence confirming the recovery to an FL ground state as a function of x. The low-temperature part of $x = 1.8$ and 2, as shown in Fig. 7(b), is fitted with
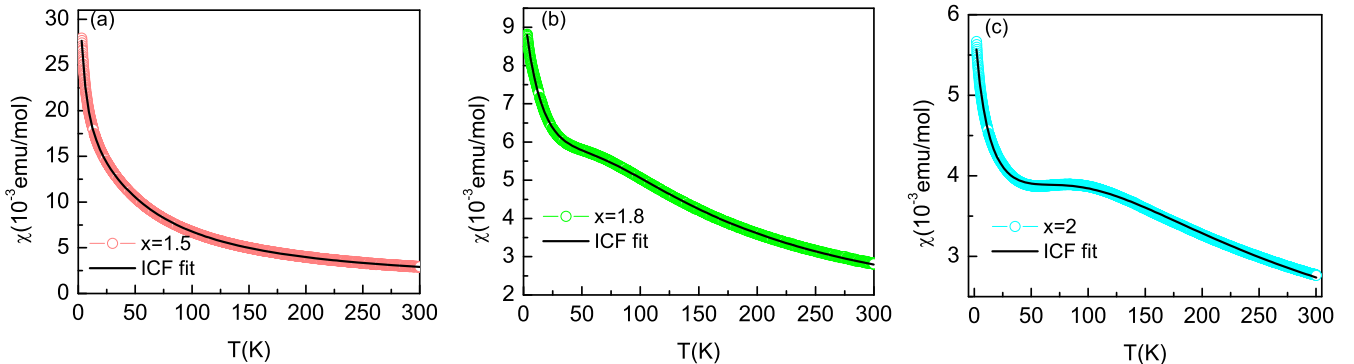
FIG. 5. Temperature-dependent magnetic susceptibility data of (a) $x = 1.5$, (b) $x = 1.8$, and (c) $x = 2$ in $CeRu_{2-x}Co_xGe_2$ measured under 100-Oe field for $x = 1.5$ and 1.8 while susceptibility data for $x = 2$ are measured under 5000 Oe, due to the weak signals. Solid lines represent the ICF model fit to the experimental data.
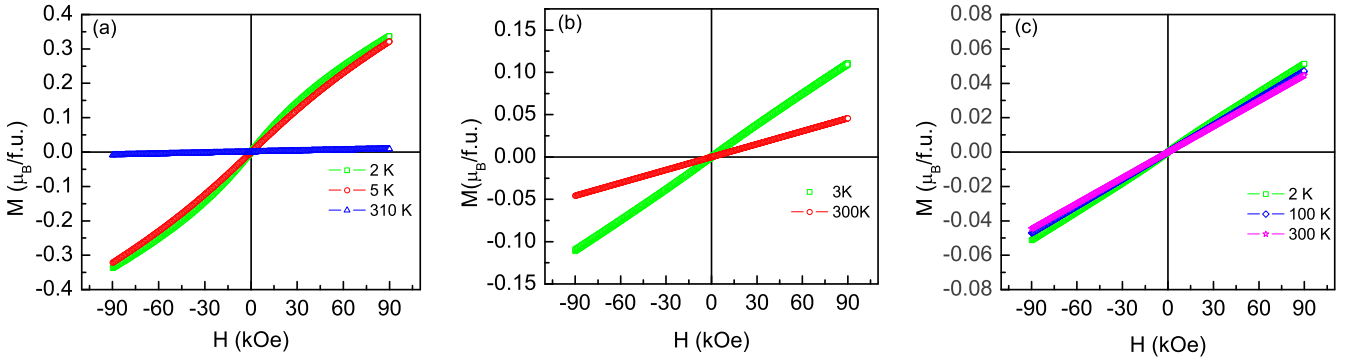
FIG. 6. Magnetization $M(H)$ vs field curves at selected temperatures for (a) $x = 1.5$, (b) $x = 1.8$, and (c) $x = 2$.

the equation $C/T = \gamma T + \beta T^2$, where γ and β represent the electron and phonon contribution, respectively. The value of γ obtained from the fit is 76.3 and 99.8 mJ/mol K^2 for $x = 1.8$ and 2, respectively, which is consistent with the Kondo screened state at low temperatures and the value obtained for $x = 2$ is in agreement with the reported result of CeCo$_2$Ge$_2$ [40]. This enhanced electronic effective mass is due to the strong coupling between the $4f$ and conduction electrons and further shows moderate heavy fermion behavior.

The magnetic resistivity ρ_m obtained by subtracting the resistivity of nonmagnetic isostructural LaCo$_2$Ge$_2$ is plotted as a function of temperature in Fig. 8(a). The nature of ρ_m curves resembles those of Ce based intermetallics such as CeIr$_2$Si$_2$ [39], CeAl$_3$, and CePd$_3$ [41], exhibiting the IVF nature. The broad maxima obtained in the resistivity curves are in line with the maxima obtained from the susceptibility measurements. This shows a negative logarithmic temperature $(-\ln T)$ behavior at higher temperatures while the sharp drop marks the onset of Kondo coherence [4] at the lower temperatures.

We tried to describe the high-temperature resistivity behavior with the model proposed by Freimuth [42] for the Ce and Yb based systems with unstable $4f$ shells. This model takes into account the scattering between s and d electrons, forming the conduction band, and the narrow $4f$ electron band. The

resistivity above 30 K in our case is fitted with the equation

$$\rho(T) = \rho_0 + aT + bJ_{SF}^2 \frac{W(T)}{T_0^2 + W(T)^2}, \quad (3)$$

where ρ_0 is the residual resistivity, the linear term in the equation gives the contribution due to electron phonon scattering with a coefficient a, T_0 is the position of the center of the $4f$ band with respect to the Fermi energy E_F, and $W(T) = T_{SF}*\exp(-T_{SF}/T)$ is the effective energy width for scattering; T_{SF} is the spin-fluctuation temperature between $4f^0$ and $4f^1$ configuration; J_{SF} is the overlap of s, d, and f electron wave functions; while b is defined as $b = m^*k_B/ne^2\hbar$ with a value of around 0.1 $\mu\Omega$ cm/K [42]. As can be seen from Fig. 8(b), the curves are fitted well with the Freimuth model. The values of the parameters obtained from the fits, listed in Table III, are consistent with the various IVF compounds [43,44]. Increase in J_{SF} with x suggests the increased overlap and hybridization between the $4f$ and conduction electrons. Again, increase in T_{SF} value with x further suggests the increased spin-fluctuation rate between 3+ and 4+ states and is in line with the susceptibility analysis. Additionally, the low-temperature part of the resistivity curves below 6 K for $x = 1.8$ and 2 is described with $\rho \sim AT^2$ dependence suggesting the FL ground state (see Fig. 9). The obtained values of the coefficients A are 1.051 and 1.109 $\mu\Omega$ cm/K^2 for $x = 1.8$ and 2, respectively.
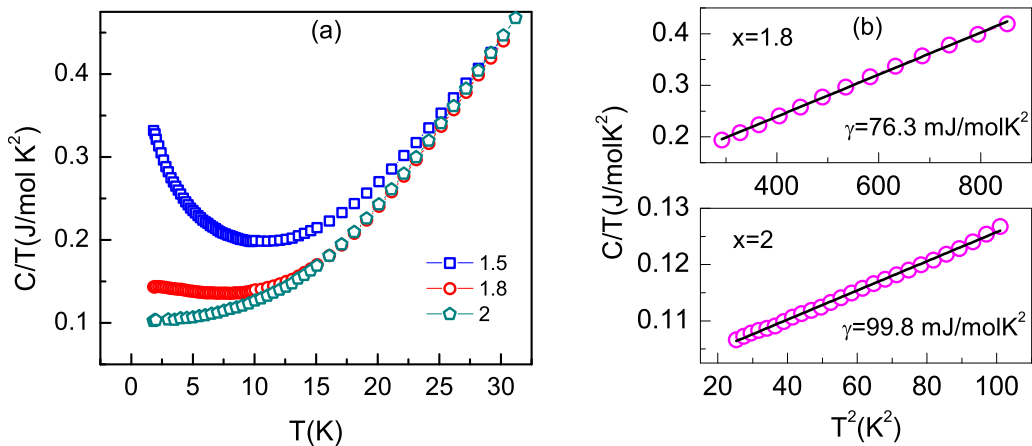
FIG. 7. (a) C/T vs T in the temperature range 1.8–30 K for concentrations $x = 1.5$, 1.8, and 2. (b) C/T against T^2 plot for $x = 1.8$ and 2 where the black line is a linear fit to the equation $C = \gamma T + \beta T^2$.
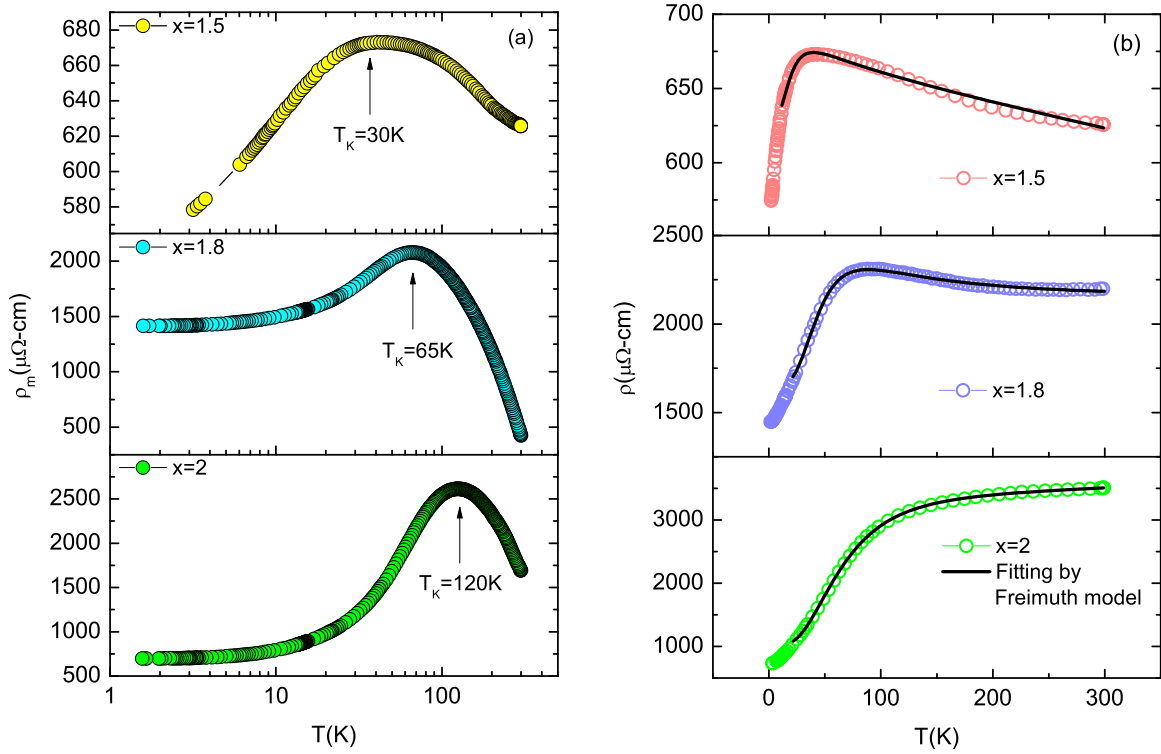
FIG. 8. (a) Magnetic resistivity ρ_m against temperature on a semilogarithmic scale for $x = 1.5$, 1.8, and 2. The Kondo temperatures (T_K) are marked by arrows. (b) High-temperature Freimuth model fitting of electrical resistivity shown by the solid lines.

C. $x = 1.5$: Non-Fermi-liquid behavior and quantum critical scaling analysis

As the pressure results in CeRu$_2$Ge$_2$ revealed a QCP close to 7 GPa [45], we suspect a doping induced QCP to occur for the present system. From the phase diagram presented below (see Fig. 15), we believe the critical concentration to be near $x_c \sim 1.5$. Figure 10(a) shows the semilogarithmic plot of $\chi(T)$ for all concentrations, $x = 0 - 2.0$. It clearly reveals that the low-temperature $\chi(T)$ for $x = 1.5$ exhibits a logarithmic dependence. The experimental data below 10 K are fitted with the $\chi(T) \propto \ln T$ term, as shown in Fig. 10(b). Moreover, it could equally be described using a power law $\chi(T) \propto T^{-1+\lambda}$ ($\lambda = 0.71$) which strongly suggests the NFL behavior [46]. Such logarithmic and power-law dependence for $\chi(T)$ is often reported for the systems near a QCP.

Figure 11(a) presents the $4f$ derived heat capacity plotted as C_{4f}/T versus $\log T$, where the phonon contribution was subtracted using the nonmagnetic compound LaCo$_2$Ge$_2$. Different behavior across three different concentration regions could clearly be identified: (a) the Ru rich region ($0 \leqslant x \leqslant 1$)

shows a clear magnetic transition, (b) $x = 1.5$ shows a pronounced upturn which suggests the possibility of a QCP, and (c) $x = 1.8$ and 2 show nonmagnetic behavior. As shown in Fig. 11(b), data in the range $2 < T < 6$ K are fitted with the term $C_{4f}/T \sim -\ln(T_0/T)$ where T_0 (~ 45 K) represents a characteristic temperature, which generally reflects the Kondo or spin-fluctuation temperature. However, the data in the extended range could also be fitted with a term proportional to $C_{4f}/T \sim T^{-1+\lambda}$ ($\lambda = 0.62$) which is in agreement with the susceptibility data as discussed above in a similar T range. The C/T on a log T scale in the presence of different

TABLE III. Fitting parameters of electrical resistivity ρ obtained from the Freimuth model. Also reported are the values of the Kondo temperature T_K.

x	T_{SF} (K)	T_0 (K)	J_{SF} (K)	T_K
1.5	35	16	130	30
1.8	92	32	647	65
2	101	69	1812	120
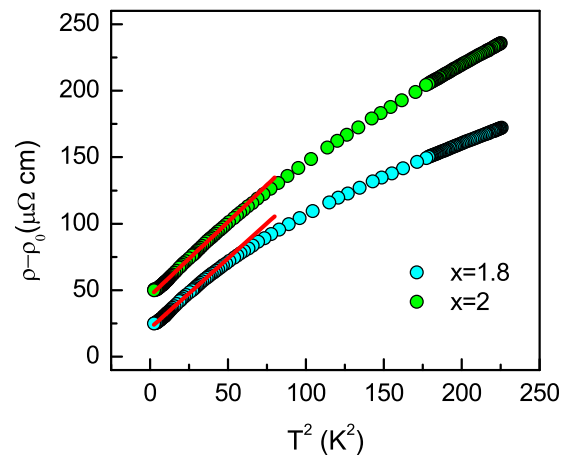
FIG. 9. $\rho - \rho_0$ vs T^2 plot at low temperatures for $x = 1.8$ and 2. The solid line fit represents the FL behavior.
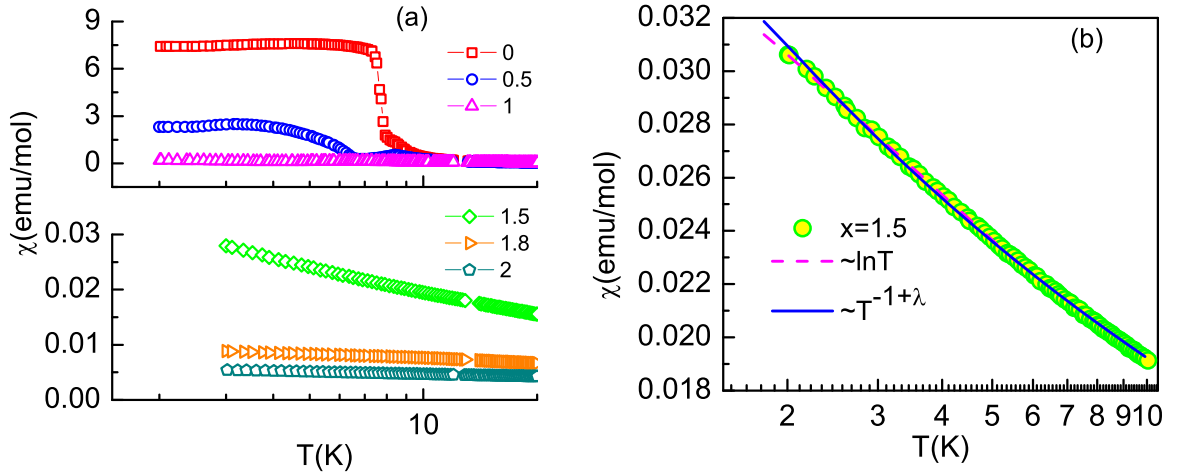
FIG. 10. (a) χ vs T on the log scale for $CeRu_{2-x}Co_xGe_2$ in which a logarithmic dependence for $x = 1.5$ can be clearly seen compared to other concentrations. (b) Data below 10 K for $x = 1.5$ show both logarithmic as well as power-law dependence.

magnetic fields for $x = 1.5$ is shown in the inset of Fig. 11(b). At zero field, there is a negative logarithmic temperature dependence below 10 K which is considered as a fingerprint of NFL behavior [47]. However, the external magnetic field suppresses the negative logarithmic divergence and at higher fields there is a crossover from NFL to FL behavior. Also, with increasing field, a maximum starts developing and shifts to a higher temperature which is likely due to Zeeman splitting of the ground crystal electric-field doublet.

Electrical resistivity ($\rho - \rho_0$) for $x = 1.5$, plotted against $T^{1/2}$ and $T^{3/2}$, for the fields 0 and 8 T is shown in Figs. 12(a) and 12(b), respectively. The low-temperature data for the respective fields are fitted with the equation $\rho = \rho_0 + AT^n$. The value of $n = 0.5$, away from $n = 2$, for 0 T suggests the deviation from the conventional FL T^2 behavior. This again confirms the NFL nature of this compound. However, the value of $n = 1.5$ for the 8-T field suggests the recovery to a FL state.

Conclusive support for a QCP is provided by the scaling analysis of temperature and field dependent magnetization as

well as resistivity for $x_c \sim 1.5$, which is located near the QCP. The curves could be collapsed onto a single universal curve following the scaling functions as discussed in Refs. [48,49]:

$$\frac{M}{H} = T^{-\eta} f\left(\frac{H}{T^\beta}\right) \text{ and } \frac{\Delta\rho}{T} = f\left(\frac{H}{T^\beta}\right). \quad (4)$$

The main panel of Fig. 13(a) represents scaled curves for the isothermal magnetization. The data could be seen to collapse onto a single curve with best scaling achieved by the choice of $\eta = 0.31$ and $\beta = 1.05$. Moreover, magnetization data measured at constant fields in the range up to 30 K and 9 T could also be scaled, as shown in the inset of Fig. 13(a). The data for susceptibility and magnetization could be seen to scale up to two decades in (H/T^β). Similar values of β and η have been reported for $CeNi_2Ge_2$, $YbRh_2Si_2$ [50,51] and $Y_{0.8}U_{0.2}Pd_3$ ($\eta = 0.3$), $UCu_{3.5}Pd_{1.5}$ ($\eta = 0.27$) [49,52] compounds, respectively. Furthermore, resistivity [$\Delta\rho(H, T) = \rho(H, T) - \rho(0, T)$] data up to 25 K and 8 T could also be scaled as a function of H/T^β [shown in Fig. 13(b)] with the same value of exponent β as obtained for
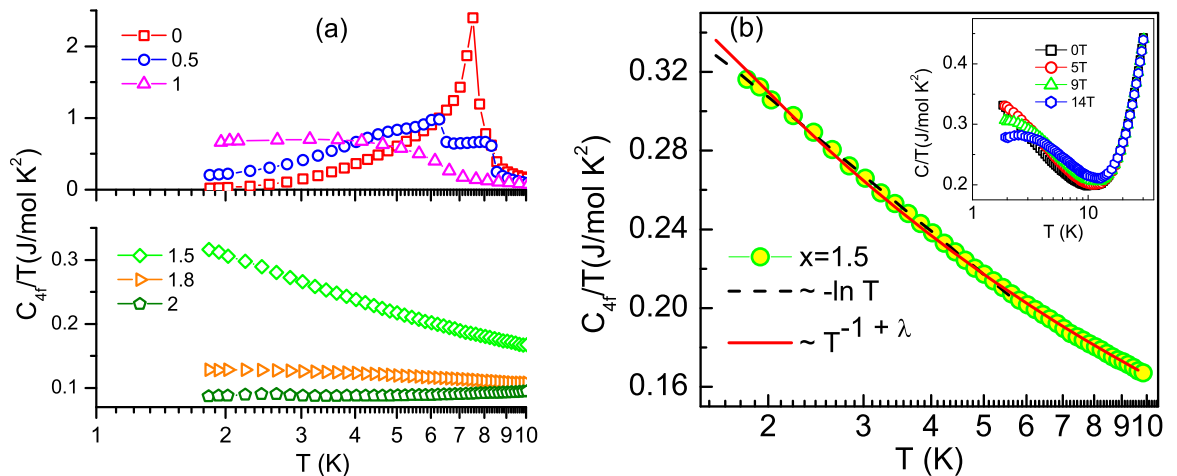
FIG. 11. (a) Semilogarithmic representation of $4f$ derived heat capacity plotted as C_{4f}/T vs T for $CeRu_{2-x}Co_xGe_2$ obtained after subtracting the heat-capacity data of reference compound $LaCo_2Ge_2$. (b) Semilogarithmic plot of C_{4f}/T for $x = 1.5$, showing both logarithmic as well as power-law dependence depicting the NFL behavior while the inset shows a plot of C/T vs $\log T$ in the presence of magnetic field.
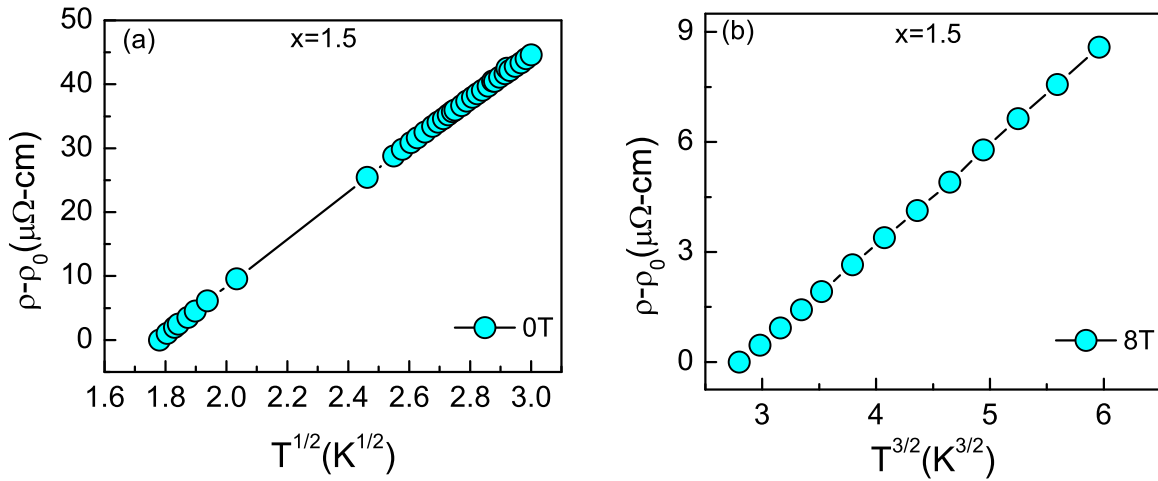
FIG. 12. (a) $T^{1/2}$ temperature dependence in the low-temperature region at 0 T for $x = 1.5$, showing the deviation from T^2 dependence and (b) $T^{3/2}$ temperature dependence at 8 T for $x = 1.5$.

magnetization and show remarkably good scaling spanning up to two decades.

IV. DISCUSSION

Further insight into the Kondo effect is gained from magnetic entropy study. The magnetic entropy calculated using $S_{mag}(T) = \int_0^T \frac{C - C_{latt}}{T} dt$ is plotted in Fig. 14. The $S_{mag}(T)$ curve for $x = 0$ continuously increases and reaches 70% of $R\ln2$ across T_C and the full value of $R\ln2$ at 19 K as expected for a well-separated crystal-field doublet ground state. However, with increase in Co concentration, entropy continuously decreases. For $x = 2$ only 30% of $R\ln2$ could be recovered up to 20 K. This suggests the Kondo effect at play, where the spins of localized Ce moments get compensated by the spins of the conduction electrons. The reduced values of entropy as well as the ordered magnetic moment of the Ce ion values of the CEF split doublet ground state suggest the role of increasing Kondo effect as a function of x. Also, the increase in strength of Kondo interaction further suggests the desta-

bilization of the Ce $4f$ moment and stronger hybridization between $4f$ and conduction electrons close to the Fermi level, which in turn leads to the valence fluctuation away from the Ce^{3+}. The overall changes as a function of x are brought about by the smaller ionic radii of Co. Given the smaller ionic radii of Co, there is a reduction in the unit-cell volume as a function of increasing Co concentration which further leads to a strong $4f$ and conduction electron hybridization [13,31].

The (T, x) phase diagram constructed using different features, viz., T_C, T_N, and T_K obtained from the magnetic susceptibility, heat capacity, and electrical resistivity, is represented in Fig. 15. The magnetic transition temperatures from all three measurements are estimated from the maxima in the respective derivative curves. Regions with different ground states as a function of doping are in agreement with the Doniach necklace model described for Kondo systems [8]. We observed a gradual decrease in T_C while T_N remains constant up to $x = 0.5$. With further increase in x, T_C disappears first followed by a complete suppression of T_N and a NFL behavior is observed in the low-temperature physical
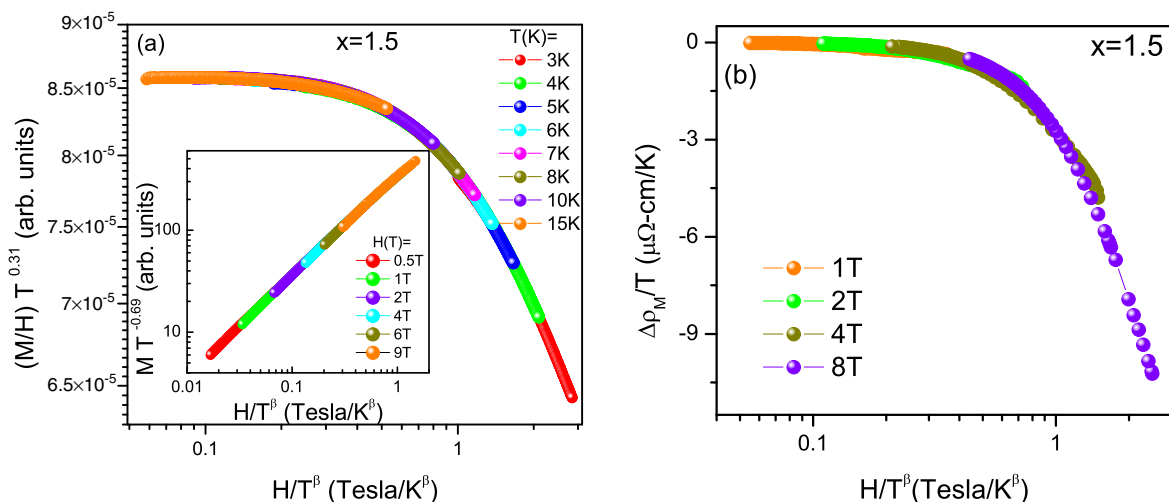
FIG. 13. (a) The main panel shows scaling collapse of isothermal magnetization while the inset shows scaling collapse of susceptibility measured at constant fields. (b) Scaling plot of resistivity in the temperature range $3 < T < 25$ K up to 8 T.
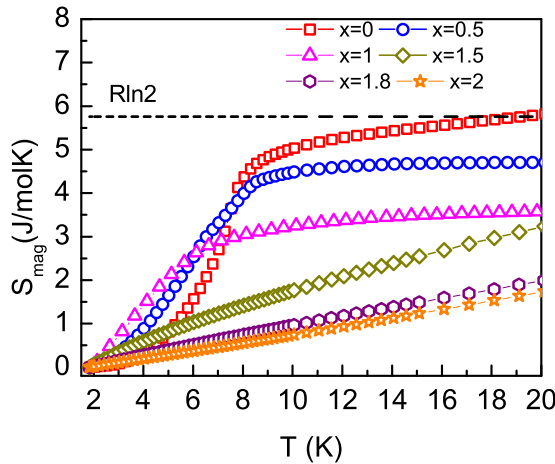
FIG. 14. Magnetic entropy as a function of temperature for the different concentrations of $CeRu_{2-x}Co_xGe_2$. The horizontal dashed line shows the value of $R\ln2$.

properties for $x = 1.5$. The experimentally observed NFL behavior for f-electron based compounds can be described by different theoretical models: (1) the Kondo disorder model [53], (2) the Griffiths phase model [54], and (3) nearness to magnetic-nonmagnetic transition at $T = 0$ K [55,56]. The $-\ln T$ behavior observed across the magnetic to nonmagnetic transition in magnetic susceptibility as well as in heat capacity indicates the magnetic QCP where quantum fluctuation governs the physical properties down to $T = 0$ K. However, keeping in mind the disorder induced as a function of doping, the power-law behavior in the extended temperature range, as well as the similarity between the λ values obtained from two different measurements, equally suggest the applicability of the Griffiths phase model. These models are appropriate for describing NFL behavior if the valence of Ce ions is considered to be $+3$. However, interestingly in view of the intermediate valence of Ce ions near and above the critical concentration $x_c \sim 1.5$, for the present case, the existence of a QCP due to transition from integral to intermediate
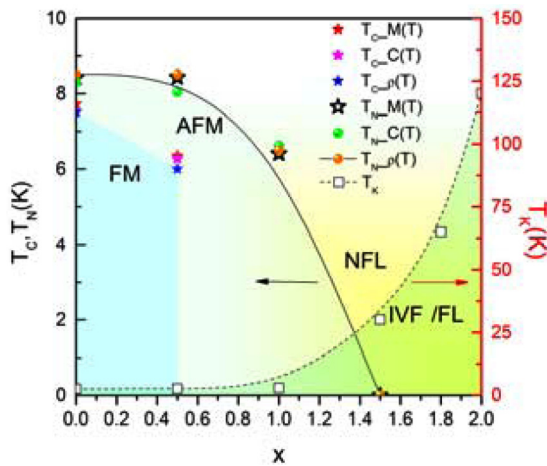
FIG. 15. (T, x) phase diagram of $CeRu_{2-x}Co_xGe_2$ summarizing the results from magnetic susceptibility (χ), heat capacity (C), and resistivity (ρ) data. The solid as well as dotted lines are guides to the eyes.

valence state may be considered. Similar behavior is observed for the case of $CeCu_2Ge_2$, $CeCu_2(Si_{1-x}Ge_x)_2$, $\beta - YbAlB_4$, and $YbCu_{5-x}Al_x$ [57–59], where the NFL behavior could be ascribed to the incipient quantum critical end point in the phase diagram. Moreover, given the valence change away from Ce^{3+}, it will be interesting to see the effect of pressure on the other end compound of the series $CeCo_2Ge_2$, whether or not the critical end point leading to the valence transition evolves further up in temperature, as a function of pressure. Also, the present paper evidences a twofold recovery to the FL ground state for the critical concentration $x_c \sim 1.5$: (a) with the application of magnetic field and (b) with the further increase in doping concentration. The FL nature for $x = 1.8$ and 2 is reflected in the low-temperature physical properties of χ, C/T, and ρ. Again the verification of the FL state for $CeCo_2Ge_2$ comes from the Kadowaki-Woods (KW) [60] ratio defined as A/γ^2 which in our case is found to be of the order of $0.11 \times 10^{-5} \, \Omega \, \text{m} \, \text{mol}^2 \, \text{K}^2/\text{J}^2$, which is compatible with the other heavy fermion and valence fluctuating compounds for which the value KW ratio ought to be $10^{-5} \, \Omega \, \text{m} \, \text{mol}^2 \, \text{K}^2/\text{J}^2$. Also, the relation between γ and χ is given by Wilson ratio R defined as $R = \frac{\pi^2 k_B^2 \chi_0}{g^2 \mu_B^2 \, J(J+1)\gamma}$ where k_B is the Boltzmann constant and g is the Landé factor. The value of the Wilson ratio for $CeCo_2Ge_2$ is about 1.87, which is in agreement with the theoretically predicted value of $R = 2$ for the spin-$\frac{1}{2}$ Kondo system [61]. A large value of γ and observation of the FL ground state indicate that $CeCo_2Ge_2$ is a heavy fermion compound with a strong hybridization between the $4f$ and conduction electrons.

V. CONCLUSIONS

Magnetic susceptibility, heat capacity, and resistivity studies investigated across the series $CeRu_{2-x}Co_xGe_2$ ($0 \leqslant x \leqslant 2$) show a smooth crossover from the RKKY dominated regime ($x < 1.5$) to a Kondo dominated regime ($x > 1.5$) as a function of doping x. This further suggests the role of unit-cell volume in stabilizing the different ground states. With the increase in strength of $4f$-conduction electron hybridization for Co rich compounds, they tend to show intermediate valence fluctuating behavior. Moreover, a doping induced QCP is evidenced around $x_c \sim 1.5$ giving NFL temperature dependence in the physical properties: C/T, χ, and ρ. However, FL behavior is recovered with increasing the doping concentration or on application of magnetic field. Existence of a QCP near $x_c \sim 1.5$ is further confirmed through the scaling analysis of magnetization and resistivity spanning over two decades in H/T^β. Furthermore, the data sets could be collapsed onto a single curve up to temperatures as high as 30 K, evidencing the non-Fermi-liquid physics governing the physical and thermodynamical properties of the system near the QCP. Even more interesting in this paper is the fact that intermediate valence fluctuation is attributed as a possible reason for the QCP observed in the case of $x_c \sim 1.5$. Only a handful of systems—to name a few, $CeCu_2Ge_2$, $\beta - YbAlB_4$, and $YbCu_{5-x}Al_x$—are studied in the light of valence fluctuation as a possible origin for the QCP. However, others were explained using different theories available in literature such as magnetic-nonmagnetic transition, Griffiths phase, Kondo disorder model, etc. Thus,

the present case adds up as a candidate to the very few similar compounds already existing and needs further experimental and theoretical studies to probe the nature and origin of QCPs.

[1] F. Steglich, J. Aarts, C. D. Bredl, W. Lieke, D. Meschede, W. Franz, and H. Schäfer, Phys. Rev. Lett. **43**, 1892 (1979).

[2] H. Kadomatsu, H. Tanaka, M. Kurisu, and H. Fujiwara, Phys. Rev. B **33**, 4799 (1986).

[3] P. Gegenwart, Q. Si, and F. Steglich, Nat. Phys. **4**, 186 (2008).

[4] J. M. Lawrence, P. S. Riseborough, and R. D. Parks, Rep. Prog. Phys. **44**, 1 (1981).

[5] D. T. Adroja and S. K. Malik, J. Magn. Magn. Mater. **100**, 126 (1991).

[6] P. Wachter, in *Handbook on the Physics and Chemistry of Rare Earths*, edited by K. A. Gschneider, Jr., L. Eyring, G. H. Lander, and G. R. Choppin, Vol. 19 (Elsevier, New York, 1994), pp. 177–382.

[7] N. B. Brandt and V. V. Moshchalkov, Adv. Phys. **33**, 373 (1984).

[8] S. Doniach, Physica B+C **91**, 231 (1977).

[9] T. Graf, J. D. Thompson, M. F. Hundley, R. Movshovich, Z. Fisk, D. Mandrus, R. A. Fisher, and N. E. Phillips, Phys. Rev. Lett. **78**, 3769 (1997).

[10] S. Kambe, S. Raymond, L. P. Regnault, J. Flouquet, P. Lejay, and P. Haen, J. Phys. Soc. Jpn. **65**, 3294 (1996).

[11] H. v. Löhneysen, T. Pietrus, G. Portisch, H. G. Schlager, A. Schröder, M. Sieck, and T. Trappmann, Phys. Rev. Lett. **72**, 3262 (1994).

[12] G. R. Stewart, Rev. Mod. Phys. **73**, 797 (2001).

[13] E. V. Sampathkumaran and R Vijayaraghavan, Phys. Rev. Lett. **56**, 2861 (1986).

[14] M. J. Besnus, J. P. Kappler, P. Lehmann, and A. Meyer, Solid State Commun. **55**, 779 (1985).

[15] L. P. Regnault, W. A. C. Erkelens, J. Rossat-Mignod, P. Lejay, and J. Flouquet, Phys. Rev. B **38**, 4481 (1988).

[16] H. Wilhelm and D. Jaccard, Solid State Commun. **106**, 239 (1998).

[17] S. Raymond, D. Raoelison, S. Kambe, L. P. Regnault, B. Fak, R. Calemczuk, J. Flouquet, P. Haen, and P. Lejay, Physica B **259–261**, 48 (1999).

[18] S. Raymond, P. Haen, R. Calemczuk, S. Kambe, B. Fak, P. Lejay, T. Fukuhara, and J. Flouquet, J. Phys.: Condens. Matter **11**, 5547 (1999).

[19] A Loidl, K. Knorr, G. Knopp, A. Krimmel, R. Caspary, A. Bohm, G. Sparn, C. Geibel, F. Steglich and A. P. Murani, Phys. Rev. B **46**, 9341 (1992).

[20] H. Fujii, E. Ueda, Y. Uwatoko, and T. Shigeoka, J. Magn. Magn. Mater. **76–77**, 179 (1988).

[21] A. P. Pikul, M. Pasturel, P. Wiśniewski, A. Soudé, O. Tougait, H. Noël, and D. Kaczorowski, Intermetallics **53**, 40 (2014).

[22] S. Süllow, M. C. Aronson, B. D. Rainford, and P. Haen, Phys. Rev. Lett. **82**, 2963 (1999).

[23] H. Wilhelm, K. Alami-Yadri, B. Revaz, and D. Jaccard, Phys. Rev. B **59**, 3651 (1999).

[24] F. Bouquet, Y. Wang, H. Wilhelm, D. Jaccard, and A. Junod, Solid State Commun. **113**, 367 (2000).

[25] T. C. Kobayashi, T. Miyazu, K. Shimizu, K. Amaya, Y. Kitaoka, Y. Ōnuki, M. Shirase, and T. Takabatake, Phys. Rev. B **57**, 5025 (1998).

[26] M. B. Fontes, M. A. Continentino, S. L. Bud'ko, M. El-Massalami, L. C. Sampaio, A. P. Guimarães, E. Baggio-Saitovitch, M. F. Hundley, and A. Lacerda, Phys. Rev. B **53**, 11678 (1996).

[27] P. Haen, H. Bioud, and T. Fukuhara, Physica B **259–261**, 85 (1999).

[28] W. Montfrooij, M. C. Aronson, B. D. Rainford, J. A. Mydosh, R. Hendrikx, T. Gortenmulder, A. P. Murani, P. Haen, I. Swainson, and A. de Visser, Phys. Rev. B **73**, 140401(R) (2006).

[29] H. Q. Yuan, F. M. Grosche, M. Deppe, C. Geibel, G. Sparn, and F. Steglich, Science **302**, 2104 (2003).

[30] D. Jaccard, K. Behnia, and J. Sierro, Phys. Lett. A **163**, 475 (1992).

[31] R. Rawat and V. G. Sathe, J. Phys.: Condens. Matter **17**, 313 (2005).

[32] D. Gignoux and J. C. Gomez-Sal, Phys. Rev. B **30**, 3967 (1984).

[33] W. C. M. Mattens, R. A. Elenbaas, and F. R. de Boer, Commun. Phys. **2**, 147 (1977).

[34] L. L. Hirst, Phys. Kondens. Mater. **11**, 255 (1970).

[35] B. C. Sales and D. K. Wohlleben, Phys. Rev. Lett. **35**, 1240 (1975).

[36] W. Franz, F. Steglich, W. Zell, D. Wohlleben, and F. Pobell, Phys. Rev. Lett. **45**, 64 (1980).

[37] Chandan Mazumdar, R. Nagarajan, S. K. Dhar, L. C. Gupta, R. Vijayaraghavan, and B. D. Padalia, Phys. Rev. B **46**, 9009 (1992).

[38] K. Hiebl, C. Horvath and P. Rogl, J. Less-Common Met. **117**, 375 (1986).

[39] B. Buffat, B. Chevalier, M. H. Tuilier, B. Lloret, and J. Etourneau, Solid State Commun. **59**, 17 (1986).

[40] T. Kong, C. E. Cunningham, V. Taufour, S. L. Bud'ko, M. L. C. Buffon, X. Lin, H. Emmons, and P. C. Canfield, J. Magn. Magn. Mater. **358–359**, 212 (2014).

[41] D. Wohlleben and B. Wittershagen, Adv. Phys. **34**, 403 (1985).

[42] A. Freimuth, J. Magn. Magn. Mater. **68**, 28 (1987).

[43] V. H. Tran, H. Flandorfer, C. Godart, and P. Rogl, J. Solid State Chem. **161**, 63 (2001).

[44] D. T. Adroja and B. D. Rainford, J. Magn. Magn. Mater. **119**, 54 (1993).

[45] A. Demuer, C. Marcenat, J. Thomasson, R. Calemczuk, B. Salce, P. Lejay, D. Braithwaite, and J. Flouquet, J. Low Temp. Phys. **120**, 245 (2000).

[46] Q. Si, S. Rabello, K. Ingersent, and J. L. Smith, Nature (London) **413**, 804 (2001).

[47] M. B. Maple, R. E. Baumbach, N. P. Butch, J. J. Hamlin, and M. Janoschek, J. Low Temp. Phys. **161**, 4 (2010).

[48] A. M. Tsvelik and M. Reizer, Phys. Rev. B **48**, 9887 (1993).

[49] B. Andraka and A. M. Tsvelik, Phys. Rev. Lett. **67**, 2886 (1991).

[50] S. Koerner, E.-W Scheidt, T. Schreiner, K. Heuser, and G. R. Stewart, J. Low Temp. Phys. **119**, 147 (2000).

[51] O. Trovarelli, C. Geibel, S. Mederle, C. Langhammer, F. M. Grosche, P. Gegenwart, M. Lang, G. Sparn, and F. Steglich, Phys. Rev. Lett. **85**, 626(2000).

[52] B. Andraka and G. R. Stewart, Phys. Rev. B **47**, 3208 (1993).

[53] O. O. Bernal, D. E. MacLaughlin, H. G. Lukefahr, and B. Andraka, Phys. Rev. Lett. **75**, 2023 (1995).

[54] A. H. Castro Neto, G. Castilla, and B. A. Jones, Phys. Rev. Lett. **81**, 3531 (1998).

[55] J. A. Hertz, Phys. Rev. B **14**, 1165 (1976).

[56] A. J. Millis, Phys. Rev. B **48**, 7183 (1993).

[57] Y. Onishi and K. Miyake, J. Phys. Soc. Jpn. **69**, 3955 (2000).

[58] S. Nakatsuji, K. Kuga, Y. Machida, T. Tayama, T. Sakakibara, Y. Karaki, H. Ishimoto, S. Yonezawa, Y. Maeno, E. Pearson, G. G. Lonzarich, L. Balicas, H. Lee, and Z. Fisk, Nat. Phys. **4**, 603 (2008).

[59] K. Yamamoto, H. Yamaoka, N. Tsujii, A. M. Vlaicu, H. Oohashi, S. Sakakura, T. Tochio, Y. Ito, A. Chainani, and S. Shin, J. Phys. Soc. Jpn. **76**, 124705 (2007).

[60] K. Kadowaki and S. B. Woods, Solid State Commun. **58**, 507 (1986).

[61] K. G. Wilson, Rev. Mod. Phys. **47**, 773 (1975).